A new Late Triassic sauropodomorph dinosaur from the Mid-Zambezi Basin, Zimbabwe

PAUL M. BARRETT, KIMBERLEY E.J. CHAPELLE, LARA SCISCIO, TIMOTHY J. BRODERICK, MICHEL ZONDO, DARLINGTON MUNYIKWA, and JONAH N. CHOINIERE

Barrett, P.M., Chapelle, K.E.J., Sciscio, L., Broderick, T.J., Zondo, M., Munyikwa, D., and Choiniere, J.N. 2024. A new Late Triassic sauropodomorph dinosaur from the Mid-Zambezi Basin, Zimbabwe. *Acta Palaeontologica Polonica* 69 (2): 227–241.

An articulated partial hind limb collected from the Pebbly Arkose Formation (Norian, Upper Triassic) of the Upper Karoo Group of Zimbabwe is described as a new taxon of sauropodomorph dinosaur. *Musankwa sanyatiensis* gen. et sp. nov. was discovered on the shoreline of Lake Kariba, on Spurwing Island in the Mid-Zambezi Basin. The holotype consists of a right femur, tibia, and astragalus, and can be distinguished from all other Late Triassic massopodan sauropodomorphs on the basis of numerous features, which form a unique character combination. Phylogenetic analysis recovers the new taxon as the earliest-branching lineage within Massopoda. *Musankwa* is only the fourth dinosaur to be named from the Karoo-aged basins of Zimbabwe and further demonstrates the high potential of this region for discoveries of new early dinosaur material.

Key words: Sauropodomorpha, Massopoda, Pebbly Arkose Formation, Norian, Lake Kariba.

Paul M. Barrett [p.barrett@nhm.ac.uk; ORCID: https://orcid.org/0000-0003-0412-3000], Fossil Reptiles, Amphibians and Birds Section, Natural History Museum, Cromwell Road, London SW7 5DB, UK and Evolutionary Studies Institute, University of the Witwatersrand, Johannesburg, Private Bag 3 Wits 2050, South Africa.
Kimberley E.J. Chapelle [kimi.chapelle@gmail.com; ORCID: https://orcid.org/0000-0002-9991-0439], Department of Anatomical Sciences, Stony Brook University, Stony Brook, New York 11794, USA; Evolutionary Studies Institute, University of the Witwatersrand, Johannesburg, Private Bag 3 Wits 2050, South Africa.
Lara Sciscio [lara.sciscio@jurassica.ch; ORCID: https://orcid.org/0000-0003-4178-2881], Jurassica Museum, Rte de Fontenais 21, 2900, Porrentruy, Switzerland; Department of Geosciences, University Fribourg, Chemin du Musée 6, 1700, Fribourg, Switzerland.
Timothy J. Broderick [makari.tim@gmail.com; ORCID: https://orcid.org/0000-0003-1891-783X], Makari, 19 Jenkinson Road, Chisipite, Harare, Zimbabwe.
Michel Zondo [michelzondo@gmail.com; ORCID: https://orcid.org/0000-0002-7918-7028], Natural History Museum of Zimbabwe, Park Road, Bulawayo, Zimbabwe; Evolutionary Studies Institute, University of the Witwatersrand, Johannesburg, Private Bag 3 Wits 2050, South Africa.
Darlington Munyikwa [dtonmunyikwa@gmail.com], National Museums and Monuments of Zimbabwe, 107 Rotten Row, Harare, Zimbabwe.
Jonah N. Choiniere [jonah.choiniere@wits.ac.za; ORCID: https://orcid.org/0000-0002-1008-0687], Evolutionary Studies Institute, University of the Witwatersrand, Johannesburg, Private Bag 3 Wits 2050, South Africa.

Received 9 August 2023, accepted 10 April 2024, published online 30 May 2024.

Introduction

Dinosaur remains from the upper part of the Stormberg Group (lower and upper Elliot and Clarens formations: Upper Triassic–Lower Jurassic; Upper Karoo Group) of the main Karoo Basin (MKB) of South Africa and Lesotho are abundant, well-studied and provide important information on the early evolution and ecology of the clade (e.g., Kitching and Raath 1984; Knoll 2004, 2005; Bordy et al. 2020; Viglietti et al. 2020a, b; and references cited therein). Similarly aged terrestrial strata are present in many of the other Karoo-aged tectonic basins that extend across southern and eastern Africa (Catuneanu et al. 2005), but these have been less thoroughly explored and their palaeontological resources require fuller documentation. For example, sedimentary sequences that are considered equivalents of

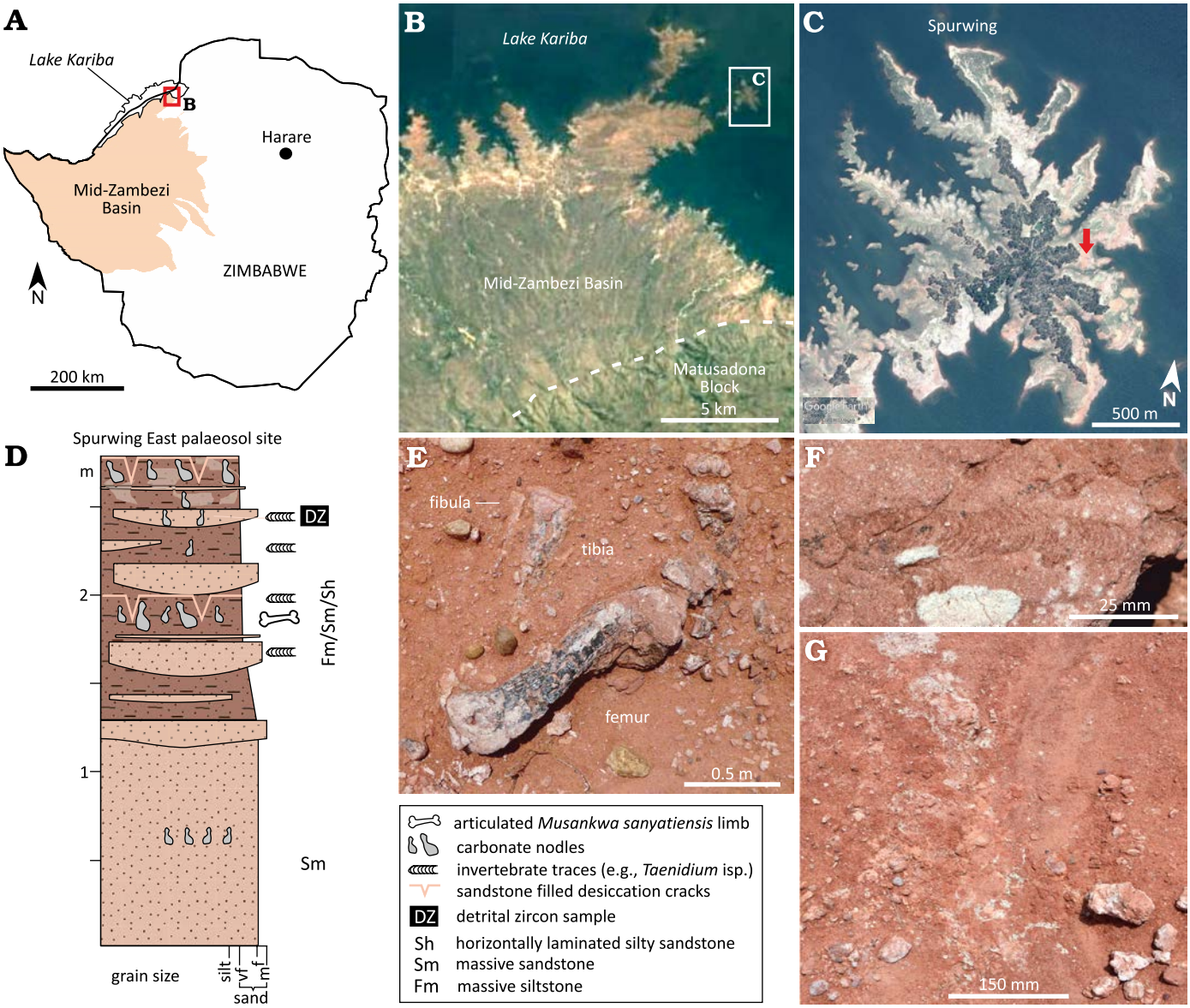

Fig. 1. **A**. Map showing the geographic setting of the Mid-Zambezi Basin in northwest Zimbabwe. **B**. Position of Spurwing Island relative to the Zimbabwean (southern) shoreline of Lake Kariba. **C**. Spurwing Island; arrow indicates the fossil locality at the Spurwing East Palaeosol site. **D**. Sedimentology of the Spurwing East Palaeosol site. **E**. Articulated hind limb of *Musankwa sanyatiensis* gen. et sp. nov. (NHMZ 2521) as discovered in situ. **F**. Evidence of bioturbation in the form of invertebrate traces (e.g., *Taenidium* isp. with menisci highlighted by red mudstone; see also Sciscio et al. 2021a). **G**. Associated sediments of the fossil site: pedogenically-modified fines with desiccation cracks, carbonate nodules, and colour mottling. Abbreviations: f, fine; m, medium; vf, very fine.

the MKB's lower/upper Elliot Formation are present in the Kalahari Karoo Basin of Botswana, the Waterberg-Erongo region of Namibia and the Mana Pools Basin of Zambia, but the former has yet to yield determinate vertebrate material (Bordy et al. 2010) and only a single dinosaur specimen has been reported from each of the two latter areas (Holzförster et al. 1999; Choiniere and Barrett 2015).

Zimbabwe hosts several Karoo-aged basins that contain Upper Karoo Group sediments, including the Tuli, Mana Pools, Cabora Bassa, and Mid-Zambezi basins (Catuneanu et al. 2005; Fig. 1A–C). Dinosaur body fossils have been reported from all of these areas, derived from either a lower series of mudstone/sandstone units, which have received numerous formation names but are generally referred to as the Pebbly Arkose Formation (or the Mpandi Formation in the Tuli Basin), or an overlying sandstone unit frequently termed the Forest (or Forest Sandstone or Samkoto) Formation (e.g., Bond 1955, 1965; Attridge 1963; Bond et al. 1970; Raath et al. 1970; Raath 1972; Bond and Falcon 1973; Cooper 1981, 1984; Munyikwa 1997; Rogers et al. 2004; Sciscio et al. 2021b; Griffin et al. 2022). These sedimentary basin fills are usually capped by flood basalts, the regional equivalents of the MKB Drakensburg Group, which provide minimum ages of ~176–186 million years for these dinosaur assemblages (Jones et al. 2001; Rogers et al. 2004; Greber et al. 2020). Lithological and faunal/floral similarities with

the Stormberg Group of the MKB led to the assumption that all these sediments were of Late Triassic–Early Jurassic age (e.g., Bond et al. 1970; Bond and Falcon 1973). However, the exact ages of the different horizons in each of these basins, as well as intra- and interbasinal correlations, have yet to be established, although one maximal depositional age for the Pebbly Arkose Formation in the Mid-Zambezi Basin is now available (209.2 ± 4.5 Ma; late Norian in Barrett et al. 2020). Moreover, there is biostratigraphic evidence that the Pebbly Arkose Formation is diachronous across these basins, as "typical" Carnian taxa, namely rhynchosaurs, have been reported from the Cabora Bassa Basin (Raath et al. 1992; Raath 1996; Griffin et al. 2022).

By far the most abundant Late Triassic–Early Jurassic dinosaur remains from Zimbabwe are those of sauropodomorphs, ranging from isolated fragments to semi-complete articulated skeletons. Historically, almost all this material has been referred to the gracile, medium-sized (up to 5 m in length and ~550 kg in body mass), bipedal taxon *Massospondylus* (e.g., Attridge 1963; Bond 1965; Raath et al. 1970; Cooper 1981; Munyikwa 1997; Rogers et al. 2004). However, to date, none of this material has been compared in detail with the more complete South African specimens on which this taxon is based (e.g., Sues et al. 2004; Chapelle and Choiniere 2018; Barrett et al. 2019). Consequently, the presence of this taxon in Zimbabwe should be regarded as tentative until more comparative work is conducted (see Barrett et al. 2019), not least as the shared presence of *Massospondylus* has been proposed as one of the primary biostratigraphic links between these sequences and those in the MKB (e.g., Bond 1965; Bond and Falcon 1973; Cooper 1982; Holzförster et al. 1999) (where *Massospondylus* is the eponymous index fossil for the latest Triassic–Early Jurassic *Massospondylus* Assemblage Zone [Viglietti et al. 2020a]). Rarer examples of more robustly built, but fragmentary, specimens have been referred to "*Euskelosaurus*" (e.g., Cooper 1980; Munyikwa 1997), which was formerly thought to be of further biostratigraphical significance (Kitching and Raath 1984), but these referrals are no longer tenable and require re-assessment, as the latter taxon is currently regarded as invalid (Yates 2003). Other sauropodomorph specimens from the Karoo-aged sediments of Zimbabwe include a partial skeleton (and other remains) of the early sauropod *Vulcanodon karibaensis*, which was excavated from a Forest Formation outcrop on the shore of Island 126/127 in Lake Kariba (Bond et al. 1970; Raath 1972; Cooper 1984; Viglietti et al. 2018), and the recently described early-diverging sauropodomorph *Mbiresaurus raathi* from the Pebbly Arkose Formation of the Dande District, in the Cabora Bassa Basin (Griffin et al. 2022). Theropod material is scarcer but represented by multiple specimens of the coelophysoid "*Syntarsus*" *rhodesiensis*, from the Forest Sandstone in the vicinity of Nyamandhlovu in the Mid-Zambezi Basin and from the Chitake River in the Mana Pools Basin (e.g., Raath 1969, 1977). Ornithischian remains are currently unknown.

Here, we describe new sauropodomorph dinosaur material from the Pebbly Arkose Formation, which was collected on Spurwing Island, Lake Kariba, Zimbabwe (Fig. 1A–C). This specimen (NHMZ 2521) represents a new massopodan taxon and adds to the diversity of dinosaurs known from the Late Triassic of this region.

Institutional abbreviations.—BP, Evolutionary Studies Institute, University of the Witwatersrand, Johannesburg, South Africa; NHMZ, Natural History Museum of Zimbabwe, Bulawayo, Zimbabwe; NMQR, National Museum, Bloemfontein, South Africa; PVL, Instituto "Miguel Lillo", Tucumán, Argentina; SAM, Iziko South African Museum, Cape Town, South Africa.

Other abbreviations.—MKB, main Karoo Basin; MPT, most parsimonious tree.

Nomenclatural acts.—This published work and the nomenclatural acts it contains have been registered in ZooBank: urn:lsid:zoobank.org:pub:5FF19455-C231-43CA-8B2E-C50F2438CCB8.

Material and methods

Sedimentological field evidence was collected by way of detailed, centimetre-scale observations of vertical and lateral facies changes using standard field techniques for sedimentary facies analysis as detailed in Miall (2006, 2010).

In order to visualise the ventral surface of the tibia and dorsal surface of the astragalus, NHMZ 2521 was scanned at the Wits Microfocus X-ray microcomputed tomography (μCT) facility in the Evolutionary Studies Institute, Palaeosciences Centre at the University of the Witwatersrand. The facility uses a Nikon Metrology XTH 225/320 LC dual source industrial μCT system. The X-ray characteristics were set at 180 kV and 180 mA, and a 2 mm thick copper filter was applied. The resulting data dimensions were as follows: 1129×1585×1725 voxels with an isotropic voxel size of 75.27 μm. Individual bones were segmented in VGSTUDIO MAX v. 3.2 (Volume Graphics, Heidelberg, Germany). 3D models (.ply) of the distal tibia and astragalus can be found in SOM 1 and 2 (Supplementary Online Material available at http://app.pan.pl/SOM/app69-Barrett_etal_SOM.pdf). Original scan data can be downloaded from MorphoSource (https://www.morphosource.org/).

As other taxa that are closely related to the new species are all obligate bipeds (see below), we assumed that the same gait was likely in our new taxon. We calculated its body mass using minimum femoral circumference (see Table 1) and the formula developed by Campione et al. (2014) for body mass estimation in bipedal taxa: Log_{10}[body mass] = 2.754 * Log10 [minimum femoral circumference] – 0.683.

NHMZ 2521 was scored as an individual operational taxonomic unit (OTU) in the phylogenetic data matrix of Pol et al. (2021). The resulting dataset contained 79 taxa

Table 1. Table of measurements (in mm); * indicate minimum measurements due to incomplete preservation.

Element	Measurement	Value
Femur	proximodistal length	428
	proximal end, maximum mediolateral width	116
	proximal end, maximum anteroposterior width	57
	lesser trochanter, total length	94*
	lesser trochanter, distance of base from proximal end of femur	157
	fourth trochanter, total length of base	54
	fourth trochanter, distance of ventral apex from proximal end of femur	180
	shaft, maximum mediolateral width at midlength	65
	shaft, maximum anteroposterior width at midlength	53
	shaft, circumference at midlength	189
	shaft, maximum anteroposterior diameter at level of lesser trochanter (excluding base of fourth trochanter)	63
	distal end, maximum mediolateral width	121*
	distal end (lateral condyle), maximum anteroposterior width	71*
Tibia	proximodistal length	365
	proximal end, maximum mediolateral width	78
	proximal end, maximum anteroposterior length	138
	cnemial crest, dorsoventral length	84
	shaft, maximum mediolateral width at midlength	40
	shaft, maximum anteroposterior width at midlength	45
	shaft, circumference at midlength	158
	distal end, maximum width anterior descending process	83
	distal end, maximum width posterior descending process	83
	distal end, maximum length	58
Astragulus	maximum mediolateral width (anterior)	92
	anteroposterior length (medial)	55
	anterior height (medial)	29 (minimum, hidden in part by tibia)
	anterior height (lateral, including ascending process)	43
	posterior height (medial)	25

and 418 equally weighted discrete morphological characters. We ordered characters following the scheme given in the original publication (see SOM 3 and 4). One character was deleted (Character 353), resulting in some changes to character numbering, and we made several minor changes to character scores (see SOM 5 for details). We analyzed the resulting matrix in TNT v. 1.5 (Goloboff and Catalano 2016), using a modified version of the protocol specified in Pol et al. (2021) including: a "traditional" search, using a random seed of 1, 1000 random addition of sequences and holding one tree per iteration. Resulting most parsimonious trees (MPTs) were subjected to an additional round of TBR branch swapping. We computed Bremer supports in TNT, examining suboptimal topologies up to five steps longer than the MPTs and holding up to 10 000 trees in memory for Bremer calculation. Strict and reduced consensus trees were calculated in TNT, and for the latter we excluded *Agnosphitys*, *Pampadromeus*, *Irisosaurus*, *Sefapanosaurus*, *Xixiposaurus*, and *Blikanasaurus* from consensus calculations, following the procedure adopted by Pol et al. (2021).

As our phylogenetic results indicate that NHMZ 2521 represents the earliest-diverging massopodan sauropodomorph (see below) we restrict our comparative observations to other closely-related taxa with an emphasis on those known from the Late Triassic of southern Africa and South America.

Geological setting

NHMZ 2521 was collected from the "Spurwing East palaeosol" site located on Spurwing Island, ~2 m from the shoreline of Lake Kariba (Fig. 1A–C). The site falls within the Pebbly Arkose Formation (Upper Karoo Group) and is likely Late Triassic (Norian) in age (Fig. 1D; Barrett et al. 2020). The sedimentology and ichnology of the site were documented in detail by Sciscio et al. (2021a, b). The material described herein (Fig. 1E) was recovered from a sandy siltstone (Fig. 1D) with a well-developed pedogenic assemblage (Fig. 1F, G). This assemblage is composed of deeply penetrative sandstone-filled desiccation cracks (laminated to massive infill), small (<4 cm-long) pedogenic carbonate nodules, evidence of bioturbation, and other palaeopedogenic alteration features such as colour mottling (Fig. 1F, G). It forms part of a ~1 m-thick unit that has thin (<20 cm-thick), interbedded, laterally discontinuous, very fine-grained to fine-grained

sandstone bodies. These can be massive, horizontally laminated, to bioturbated. Bioturbation is more common and of a higher intensity within the interbedded sandstone lenses than in the finer-grained host medium.

Overall, the site provides evidence for overbank deposition that is periodically and repeatedly punctuated by higher-energy events that deposit muddy sandstone sheets. Repeated wetting-drying and subaerial exposure are demonstrated by the desiccation cracks, pedogenic mottling, and invertebrate trace fossils.

Systematic palaeontology

Sauropodomorpha Huene, 1932

Massopoda Yates, 2007

Genus *Musankwa* nov.

ZooBank LCID: urn:lsid:zoobank.org:act:1671E607-6DC5-4977-B394-B96375911BDE

Etymology: In reference to the house-boat "Musankwa", from the Tonga dialect, meaning "boy close to marriage"; see SOM 5: fig. S1. This vessel acted as our home and mobile laboratory during two field expeditions to Lake Kariba in 2017–2018, and was made available through the generosity of David and Julie Glynn. Its crew, Coster Katupu, Godfrey Swalika, Simbarashe Mangoroma, and Never Mapira, provided essential logistic support.

Type species: *Musankwa sanyatiensis* sp. nov., by monotypy, see below.

Diagnosis.—As for the type species, see below.

Musankwa sanyatiensis sp. nov.

Figs. 1E, 2, 3.

ZooBank LCID: urn:lsid:zoobank.org:act:A0C7FA6C-0A14-40F1-97E1-621F99D81AE3

Etymology: Named for the Sanyati River, whose original course is now submerged in the Sanyati Basin of Lake Kariba, in which the type locality (Spurwing Island) is situated.

Holotype: NHMZ 2521, a partial right hind limb, consisting of a complete femur, tibia, and astragalus, with associated indeterminate bone fragments.

Type locality: The "Spurwing East Palaeosol" site (16°43.592'S, 28°41.771'E; Fig. 1; see also Sciscio et al. 2021b), situated on the north-eastern shoreline of Spurwing Island, Lake Kariba, Zimbabwe (Mid-Zambezi Basin).

Type horizon: Pebbly Arkose Formation, Upper Karoo Group, Norian, Upper Triassic (see Barrett et al. 2020; Sciscio et al. 2021b).

Diagnosis.—Prominent posterior tubercle present on proximal margin of femur (also present in *Eucnemesaurus*, *Riojasaurus*, and *Sefapanosaurus*); shaft of proximal femur anteroposteriorly expanded and swollen at the level of the anterior trochanter (also in *Coloradisaurus*, absent in other taxa); base of fourth trochanter straight, positioned centrally on the posterior surface of the femur, and situated entirely within the proximal half of the femur (unique character combination, absent from other taxa); fibular condyle of proximal tibia separated from the cnemial crest by a distinct sulcus (also in *Coloradisaurus*).

Material.—Type material only.

Description.—The specimen described herein was discovered by one of us (PMB) during an expedition to the southern shore of Lake Kariba in March 2018 (see also Sciscio et al. 2021a; Barrett et al. 2023; Fig. 1A–C). It was found weathering out on the surface with the preserved elements in articulation (Fig. 1E). The material is heavily sun-cracked and weathered, with poor surface preservation that might reflect a long period of surface exposure prior to collection, as well as pre-burial damage. No other vertebrate material was found in the immediate vicinity of the find. The holotype consists of a partial right leg (Figs. 1E, 2, 3) including a femur, tibia, and astragalus, all of which are largely complete, and small indeterminate bone fragments. The astragalus remains in articulation with the distal tibia. The tibia is shorter than the femur, reaching ~85% of the length of the latter. Measurements for all the elements are provided in Table 1. Based on the formula for inferring body mass for bipedal taxa using minimum femoral circumference (see Material and methods above), NHMZ 2521 has an estimated body mass of ~386 kg.

Femur: In anterior view, the femur is strongly sigmoidal in outline, with the shaft twisting laterally below the level of the proximal end, then strongly medially at midlength, and finally twisting laterally in its ventral-most part (Fig. $2A_1$). It is also subtly sigmoidal in lateral view, although the degree of twisting in this plane is much less pronounced, with the shaft bowing posteriorly just ventral to the dorsal end as well as distally, and bowing anteriorly in its dorsal-most and central parts (Fig. $2A_2$).

The head of the femur is oriented medially and slightly ventrally in anterior view (Fig. $2A_1$). It has a rounded, semicircular outline, but poor preservation makes interpretation of other features difficult. For example, there appears to be a distinct ligament groove on the anterior surface extending parallel to the medial margin of the process, but this could be the result of erosion or damage as there is no cortical bone in this area. The ventral margin of the femoral head is separated from the shaft by an angle of ~120° and the two surfaces grade into each other without an abrupt change in slope. In medial view, the head has a sub-oval outline that is broadest dorsally and tapers to a rounded apex ventrally (Fig. $2A_4$).

In anterior view, the greater trochanter is situated slightly dorsal to the level of the femoral head. Its lateral margin is gently curved and meets the dorsal surface at ~90°. Its dorsal margin forms a continuous straight line with that of the femoral head. The entire proximal end of the femur is twisted with respect to the shaft, so that the femoral head projects strongly anteromedially, a feature best observed in proximal view. Overall, in proximal view, the dorsal surface of the femur has a sub-elliptical outline that is anteroposteriorly expanded in its central part (at the level of the posterior tubercle) and tapers laterally and medially, with the femoral head exhibiting greater expansion than the greater trochanter (Fig. $2A_5$). The dorsal surfaces of the femoral head and greater trochanter are confluent and there is no fossa tro-

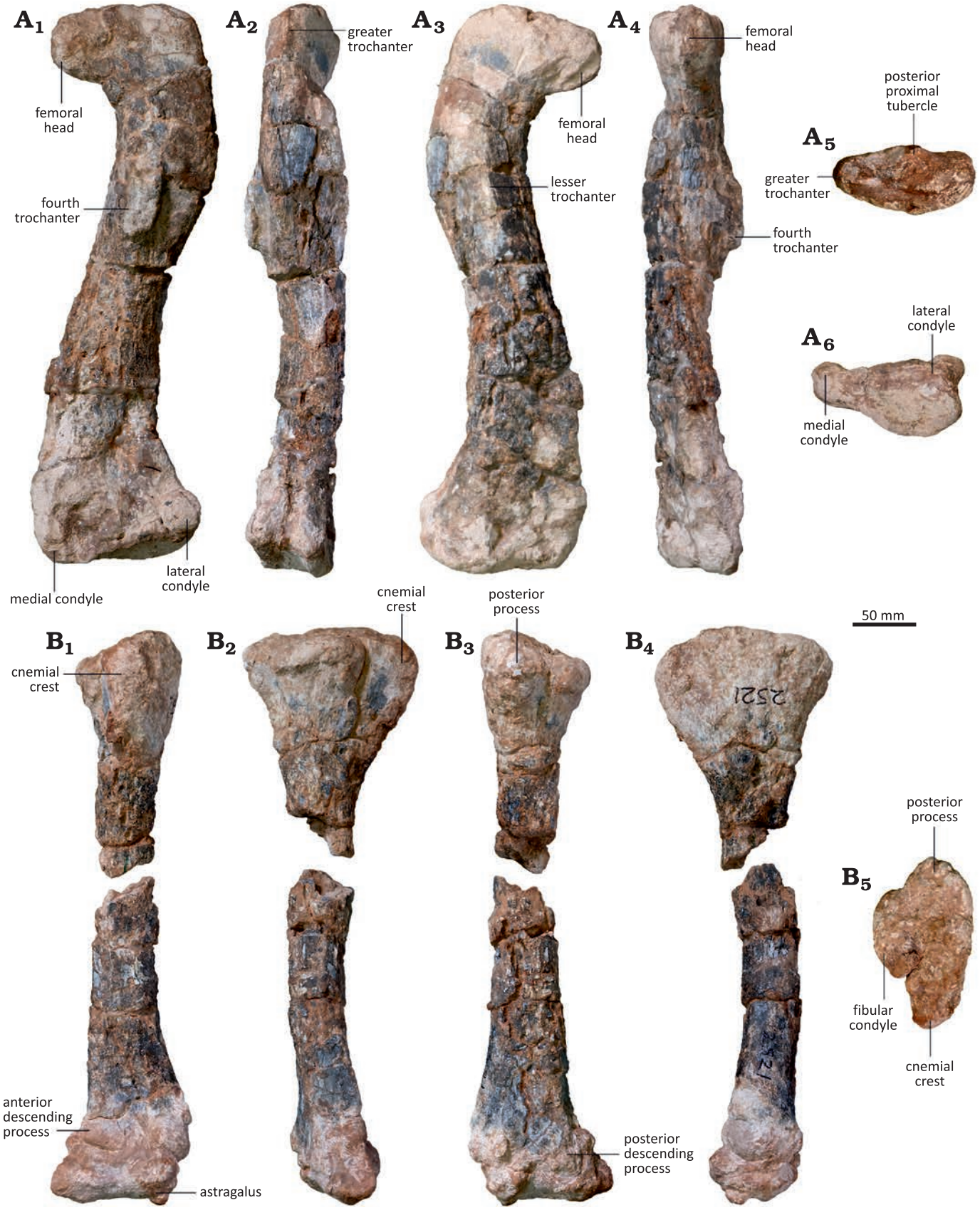

Fig. 2. Right hind limb of the sauropodomorph dinosaur *Musankwa sanyatiensis* gen. et sp. nov. (NHMZ 2521) from the Pebbly Arkose Formation (Norian, Upper Triassic) of Spurwing Island, Zimbabwe. **A**. Right femur in posterior (A_1), lateral (A_2), anterior (A_3), medial (A_4), proximal (A_5), and distal (A_6) views. **B**. Right tibia with conjoined astragalus in anterior (B_1), lateral (B_2), posterior (B_3), medial (B_4), and proximal (B_5) views.

chantericus. This combined surface is gently convex both anteroposteriorly and mediolaterally, and appears to have been strongly rugose. An elliptical boss, with its long axis extending dorsomedially–anterolaterally, is positioned in the central part of the posterior surface of the proximal end, confluent with its proximal margin, and likely represents the posterior proximal tubercle (Fig. 2A$_1$, A$_5$).

A prominent, raised ridge on the anterior surface of the proximal end represents the lesser trochanter (Fig. 2A$_3$). It is situated centrally, equally distanced from the medial and lateral shaft margins. Consequently, it is not visible in posterior view. Although its dorsal apex is eroded, the remaining part indicates that it terminated well below the level of the femoral head. The process extends for a considerable distance ventrally, merging into the shaft at a point approximately 36% of the distance from the femoral dorsal margin and it extends for at least ~22% of total femoral length. The lesser trochanter is so prominent, being approximately as high as it is wide, that it imparts a strongly triangular, swollen cross-section to the proximal part of the femoral shaft (Fig. 2A$_2$, A$_4$).

The broken base of the fourth trochanter is a prominent feature positioned on the posterior surface of the shaft, slightly offset towards its medial margin (Fig. 2A$_1$). It has an elongate, elliptical outline whose long axis extends dorsoventrally. Its ventral margin is situated well above femoral midlength (and ventral to the ventral-most extent of the lesser trochanter) at around 42% of total femoral length. As broken, it is not possible to determine the shape or extent of the process. The shaft transverse cross-section ventral to the fourth trochanter is elliptical, with its longest axis oriented mediolaterally.

In anterior view, the ventral part of the femur is expanded mediolaterally with respect to the shaft, but this expansion is asymmetrical and occurs solely on its lateral side (Fig. 2A$_3$). Consequently, the medial margin of the ventral end is gently convex, forming an angle of around 90° with the femoral ventral margin, whereas the corresponding lateral margin is concave and forms an angle of around 70° with the ventral margin. Its anterior surface is flat to gently convex and lacks any fossae or ridges. The ventral margin is straight and oriented horizontally. The lateral condyle projects strictly posteriorly in both lateral and posterior views. It is shorter anteroposteriorly than it is either tall dorsoventrally or wide mediolaterally and has a sub-circular outline in posterior view, although this has likely been altered by weathering. It is separated from the medial condyle by a wide, shallow intercondylar groove. The broken base of the medial condyle indicates that it was considerably larger than the lateral condyle in both width and height, but no other details can be determined. In distal view, the preserved part of the ventral end has a sub-rectangular outline and is concave mediolaterally, but this area has been altered by damage (Fig. 2A$_6$).

Tibia: The dorsal and ventral ends of the tibia are expanded with respect to the slender elongate shaft (Fig. 2B$_1$–B$_4$). The dorsal expansion has its long axis oriented anteroposteriorly; by contrast, the ventral expansion has undergone torsion and its long axis is oriented anterolaterally-posteromedially, and this is offset by ~40–50° from that of the dorsal end.

In proximal view, the dorsal end is rugose and has a sub-triangular outline, with the apices of this triangle formed by the cnemial crest anteriorly, the fibular crest laterally, and the posterior process (Fig. 2B$_5$). The dorsal surface is anteroposteriorly convex but mediolaterally concave, so that it is very subtly "saddle-shaped". The cnemial crest is narrow and triangular in outline, being slightly longer than wide. Its apex is oriented anteriorly and very slightly laterally and has a blunt, rounded terminus. The cnemial crest is separated from the fibular condyle by a broad, open notch, which forms an angle of ~160° between the two processes. The fibular condyle has an elongate, elliptical outline that is more than twice as long as it is broad. The posterior margin of the fibular condyle meets the posterior process at an angle of ~120° forming a clearly differentiated notch between them. The posterior process has a squat, equilateral triangle-shaped outline whose apex projects posteriorly. In proximal view, the medial margin of the dorsal end describes a shallow, smoothly convex curve in contrast to the strongly sinuous lateral margin (Fig. 2B$_5$).

The dorsal end of the tibia is strongly expanded anteroposteriorly with respect to the shaft, with this expansion being almost symmetrical in either lateral or medial view (Fig. 2B$_2$, B$_4$). The cnemial crest extends for only a short distance along the anterior margin of the shaft, accounting for 18% of total tibial length, and gives the dorsal expansion a gently convex anterior margin. By contrast, the posteroventral margin of the posterior process has a more acute outline (Fig. 2B$_2$, B$_4$). The medial surface of the dorsal expansion is anteroposteriorly convex. In lateral view, the fibular condyle is supported by a stout buttress, delimited anteriorly and posteriorly by broad grooves confluent with the notches on the dorsal surface (see above), which extends for a short distance ventrally before merging into the shaft (Fig. 2B$_2$). The tibial shaft has a sub-circular transverse cross-section that is slightly wider mediolaterally than long anteroposteriorly.

The ventral surface of the tibia is obscured by the astragalus but is visible in our μCT segmentations. It has a sub-rectangular outline, which was longer anterolaterally-posteromedially than perpendicular to this (Figs. 2B$_2$, B$_3$, 3A, B). The anterior and posterior descending processes are almost identical in anterolateral-posteromedial width, but the posterior descending process extends further ventrally, creating a distinct, anterolaterally directed notch for the reception of the ascending process of the astragalus (Fig. 3B). The anteromedially facing surface of the ventral expansion is the broadest and is shallowly concave, the narrow anterolaterally facing surface is flat, and the posteromedial and posterolateral surfaces merge into each other to form a smooth, rounded surface.

Astragalus: The astragalus is tightly appressed to the tibia, obscuring its dorsal surface, although this is visible in the μCT scans (see SOM 1 and 2). In anterior view, it has

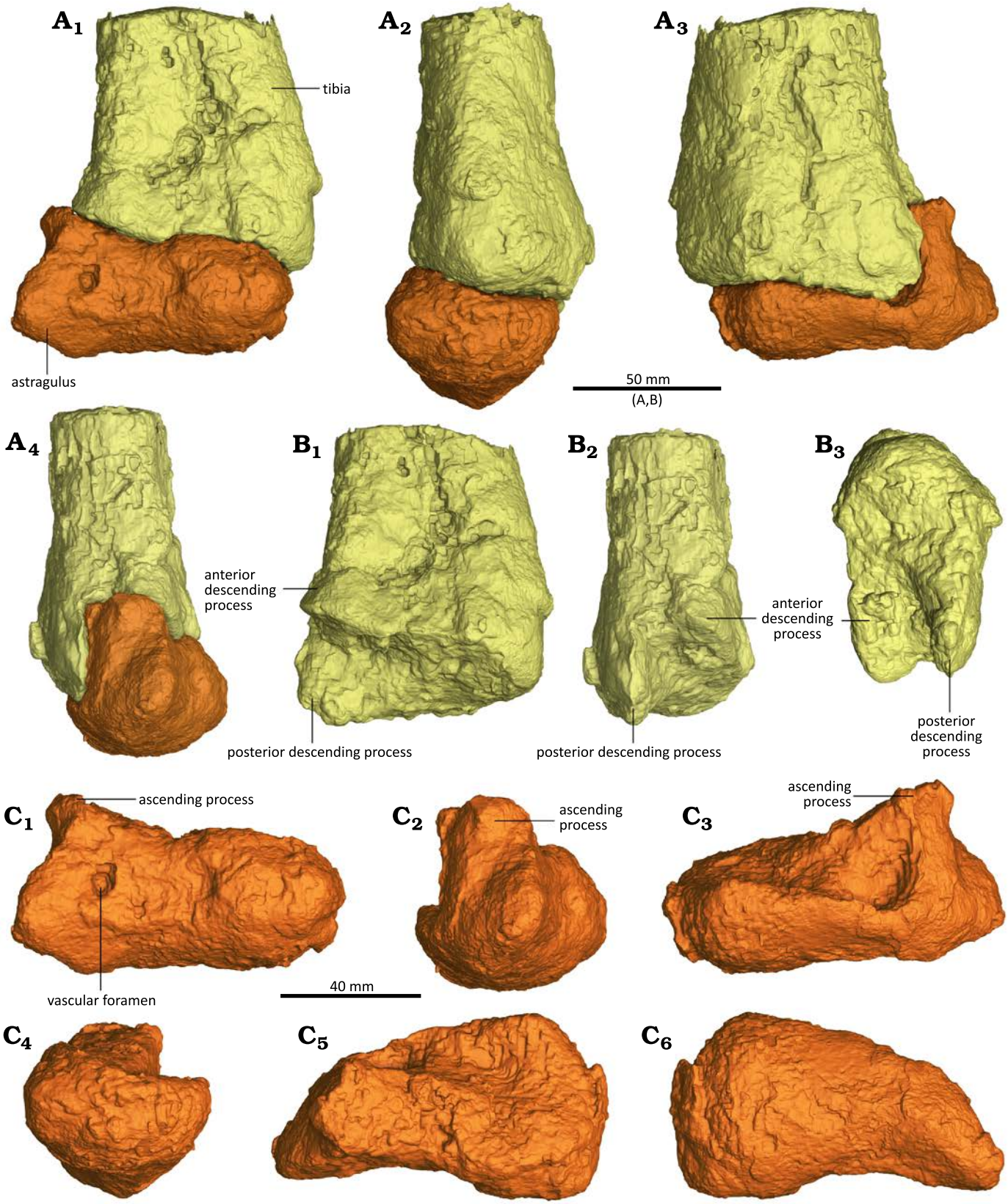

Fig. 3. CT-renderings of the distal end of the right tibia and right astragalus of the sauropodomorph dinosaur *Musankwa sanyatiensis* gen. et sp. nov. (NHMZ 2521) from the Pebbly Arkose Formation (Norian, Upper Triassic) of Spurwing Island, Zimbabwe. **A**. Articulated distal right tibia and right astragalus in anterior (A_1), medial (A_2), posterior (A_3), and lateral (A_4) views. **B**. Distal right tibia with astragalus removed digitally in anterior (B_1), lateral (B_2), and distal (B_3) views. **C**. Right astragalus digitally dissected from tibia in anterior (C_1), lateral (C_2), posterior (C_3), medial (C_4), dorsal (C_5), and ventral (C_6) views. 3D versions of these images can be found in the SOM 1 and 2 (Supplementary Online Material available at http://app.pan.pl/SOM/app69-Barrett_etal_SOM.pdf).

a sub-trapezoidal outline, whose ventral and dorsal margins are subequal in length and approximately 3.2 times longer than its medial margin is tall (Fig. 3C$_1$). The medial margin is gently convex, while all of the other margins are concave. The astragalus is dorsoventrally tallest laterally as it includes a prominent, triangular ascending process that articulates with the notch on the distal tibia (Fig. 3C$_1$, C$_2$). In anterior view, the base of the ascending process is slightly wider than it is tall. It is inset from the lateral margin of the astragalar body by a distinct notch. The lateral margin of the ascending process is oriented almost vertically and is slightly concave, whereas the medial margin slopes ventrally from the apex of the process at an angle of approximately 30º below the horizonal. A foramen is present on the anterior surface of the astragalus ventral to the ascending process, but is not set within a distinct fossa (Fig. 3C$_1$).

Most of the dorsal surface medial to the ascending process forms a large, ovate, shallowly concave articular facet for the reception of the tibia (Fig. 3C$_3$, C$_5$). This facet is anteroposteriorly broadest medially and tapers laterally as it merges with the medial surface of the ascending process. The tibial facet is inclined so that it faces posterodorsally and is highest anteriorly in medial view, while its posterior margin is formed by a slightly upturned lip. The medial slope of the ascending process is broad (accounting for approximately half of the anteroposterior length of the astragalus) and forms a planar smooth surface. This process has a triangular transverse cross-section. A distinct break-of-slope is present between the articular facet and a deep concavity that excavates the posterior margin of the ascending process.

In medial view, the astragalus has a sub-crescentic outline and the anterior, ventral, and posterior margins form a continuous convex curve (Fig. 3C$_4$). Its dorsal margin is concave for the reception of the tibia and the lateral surface is convex both anteroposteriorly and dorsoventrally. In ventral view, its articular surface is sub-rectangular in outline and its posterolateroventral corner appears to be damaged. The ventral surface is roller-like and strongly convex anteroposteriorly (Fig. 3C$_6$).

Posteriorly, the main body of the astragalus is tallest medially and tapers laterally, due to lateromedial sloping of its dorsal surface (Fig. 3C$_3$). The posterior margin of the ascending process is buttressed by a stout, vertical, robust ridge. Medial to this ridge the posteromedial margin of the process is excavated by a deep concavity.

Other material: A small part of the distal fibula was originally present (Fig. 1E) but was so poorly-preserved it did not survive collection and preparation. Several other small bone fragments were collected from around the articulated specimen, but none of these can be matched with existing breaks or have sufficient morphology to be identified further.

Remarks.—Musankwa sanyatiensis gen. et sp. nov. can be distinguished from other Late Triassic massopodan taxa on the basis of numerous hind limb characteristics. For example, the femora of *Coloradisaurus brevis* Bonaparte, 1978 (Apaldetti et al. 2013), *Kholumolumo ellenbergerorum* Peyre de Fabrègues & Allain, 2020 (Peyre de Fabrègues and Allain 2020), *Macrocollum itaquii* Müller et al., 2018 (Müller et al. 2018), *Meroktenos thabanensis* (Gauffre, 1993) (Peyre de Fabrègues and Allain 2016), *Mussaurus patagonicus* Bonaparte & Vince, 1979 (Otero and Pol 2013), and *Riojasaurus incertus* Bonaparte, 1971 (PVL 3808; Bonaparte 1971) are straight in anterior view, lacking the marked sigmoidal curvature present in *Musankwa sanyatiensis*. The femur of *Eucnemesaurus entaxonis* McPhee et al., 2015, has an intermediate condition where it is curved in its proximal part but straight distally (BP/1/6234; McPhee et al. 2015) and the partial proximal femora of *Sefapanosaurus zastronensis* Otero et al., 2015, are straight (BP/1/7440, 7441, 7442; Otero et al. 2015), differing from the strongly sigmoidal profile in *Musanwka sanyatiensis*. However, moderately sigmoidal femora are present in *Plateosauravus cullingworthi* Haughton, 1924 (Haughton 1924). The ratios of tibia/femur total length also vary among these taxa, but comparative statements are difficult due to either breakage, specimen incompleteness, or lack of definitive association. Where available these range from 0.73 in *Mussaurus patagonicus* (Otero and Pol 2013) through 0.85 in *Musankwa sanyatiensis* (Table 1) and *Riojasaurus incertus* (Bonaparte 1971), 0.87 in *Coloradisaurus brevis* (Apaldetti et al. 2013) and ~0.9 in *Macrocollum itaquii* (Müller et al. 2018).

A prominent posterior tubercle is present on the proximal femur in *Musankwa sanyatiensis*, *Eucnemesaurus fortis* Van Hoepen, 1920 (BP/1/6111; Yates 2007), *Eucnemesaurus entaxonis* (BP/1/6234; McPhee et al. 2015), and *Riojasaurus incertus* (PVL 3808), is variably present in *Sefapanosaurus zastronensis* (present in BP/1/7441 and 7442 and absent in BP/1/7440; contra Otero et al. 2015), and absent in *Coloradisaurus brevis* (Apaldetti et al. 2013), *Kholumolumo ellenbergerorum* (Peyre de Fabrègues and Allain 2016), *Meroktenos thabanensis* (Peyre de Fabrègues and Allain 2020), and *Mussaurus patagonicus* (Otero and Pol 2013). In *Musankwa sanyatiensis* and *Coloradisaurus brevis* (Apaldetti et al. 2013), the area supporting the lesser trochanter is inflated anteroposteriorly, creating a distinctive bulging of this area in lateral or medial view, and the ratio of femoral anteroposterior diameter in this region (at the base of the lesser trochanter) to femoral length is 0.15 in both taxa. This compares with the more anteroposteriorly compressed femora of *Eucnemesaurus entaxonis* (BP/1/6234; 0.11), *Kholumolumo ellenbergerorum* (Peyre de Fabrègues and Allain 2020; 0.10), *Meroktenos thabanensis* (Peyre de Fabrègues and Allain 2016; 0.10), *Mussaurus patagonicus* (Otero and Pol 2013; 0.10), and *Riojasaurus incertus* (PVL 3808; 0.11), which lack this bulge. Although it is not possible to calculate this ratio in *Eucnemesaurus fortis* and *Sefapanosaurus zastronensis* due to incompleteness (BP/1/6111, Yates 2007; BP/1/7440–7442, Otero and Pol 2013), or in *Macrocollum itaquii* due to a lack of published measurements (Müller et al. 2018), these specimens also lack the distinct swollen area present in *Musankwa sanyatiensis* and *Coloradisaurus brevis*.

In *Kholumolumo ellenbergerorum* (Peyre de Fabrègues and Allain 2020), *Meroktenos thabanensis* (Peyre de Fabrègues and Allain 2016), and *Plateosauravus cullingworthi* (Haughton 1924) the ventral part of the fourth trochanter extends onto the distal half of the femoral shaft, whereas in *Coloradisaurus brevis* (Apaldetti et al. 2013), *Eucnemesaurus entaxonis* (BP/1/6234; McPhee et al. 2015), *Macrocollum itaquii* (Müller et al. 2018), *Musankwa sanyatiensis*, *Mussaurus patagonicus* (Otero and Pol 2013), and *Riojasaurus incertus* (PVL 3808; Bonaparte 1971) this process is confined to its proximal half. Furthermore, the base of the fourth trochanter is inset from the medial margin of the femur in *Musankwa sanyatiensis* to lie almost centrally on the shaft, as in *Kholumolumo ellenbergerorum* (Peyre de Fabrègues and Allain 2020) and *Plateosauravus cullingworthi* (Haughton 1924), whereas it is medially displaced in *Coloradisaurus brevis* (Apaldetti et al. 2013), *Eucnemesaurus entaxonis* (BP/1/6234; McPhee et al. 2015), *Eucnemesaurus fortis* (BP/1/6111; Yates 2007), *Meroktenos thabanensis* (Peyre de Fabrègues and Allain 2016), *Mussaurus patagonicus* (Otero and Pol 2013), and *Riojasaurus incertus* (PVL 3808; Bonaparte 1971). In addition, the base of the fourth trochanter in *Coloradisaurus brevis* (Apaldetti et al. 2013), *Musankwa sanyatiensis*, *Kholumolumo ellenbergerorum* (Peyre de Fabrègues and Allain 2020), and *Mussaurus patagonicus* (Otero and Pol 2013) is almost vertically inclined and straight, whereas in *Eucnemesaurus fortis* (BP/1/6111; Yates 2007), *Eucnemesaurus entaxonis* (BP/1/6234; McPhee et al. 2015), *Meroktenos thabanensis* (Peyre de Fabrègues and Allain 2016), and *Riojasaurus incertus* (PVL 3808) the base is obliquely inclined, trending proximomedially–distolaterally, and often curved or kinked along its length. In *Plateosauravus cullingworthi* the base of the trochanter is curved, but its long axis is more vertically inclined (Haughton 1924).

In distal view, the lateral margin of the femur bears a shallow sulcus in *Musankwa sanyatiensis* and *Meroktenos thabanensis* (Peyre de Fabrègues and Allain 2016). A similarly positioned but deeper sulcus is present in *Coloradisaurus brevis* (Apaldetti et al. 2013), *Eucnemesaurus fortis* (BP/1/6111; Yates 2007), and *Riojasaurus incertus* (PVL 3808), but this feature is absent in *Kholumolumo ellenbergerorum* (Peyre de Fabrègues and Allain 2020).

The ratio between the maximum anteroposterior length of the proximal end of the tibia and overall tibia length varies among Late Triassic sauropodomorph taxa, from the most slender in *Jaklapallisaurus asymmetricus* Novas et al., 2011 (0.24, Ezcurra et al. 2023), though intermediate values in *Coloradisaurus brevis* (0.29, Apaldetti et al. 2013), *Eucnemesaurus fortis* (0.33, Van Hoepen 1920), *Kholumolumo ellenbergerorum*, *Musankwa sanyatiensis*, *Mussaurus patagonicus*, *Riojasaurus incertus* (0.38, in all taxa, measurements from Peyre de Fabrègues and Allain 2020, Table 1, Otero and Pol 2013, PVL 3808, respectively), *Plateosauravus cullingworthi* (0.40, Haughton 1924), and *Melanorosaurus readi* Haughton, 1924 (0.43, SAM-PK-3449; Haughton 1924), to the stockiest in *Blikanasaurus cromptoni* Galton & Van Heerden, 1985 (0.48, Galton and Van Heerden 1985).

In *Musankwa sanyatiensis*, the proximal end of the tibia has a maximum length/maximum width ratio of 1.65, which compares with the slightly more elongate proximal tibiae of *Blikanasaurus cromptoni* (1.75, SAM-PK-K403), *Kholumolumo ellenbergerorum* (1.72, Peyre de Fabrègues and Allain 2020), *Melanorosaurus readi* (1.68, SAM-PK-3449), *Plateosauravus cullingworthi* (1.77, Haughton 1924), *Riojasaurus incertus* (1.75, PVL 3808), and *Sefapanosaurus zastronensis* (1.85, BP/1/7445; Otero et al. 2015), and the stouter tibiae of *Jaklapallisaurus asymmetricus* (1.32, Ezcurra et al. 2023) and *Eucnemesaurus fortis* (1.51, Van Hoepen 1920). In addition, the fibular condyle of the tibia is a distinct process that is separated from the cnemial crest (and often the posterior process also) by a distinct sulcus or notch in *Macrocollum itaquii* (Müller et al. 2018), *Musankwa sanyatiensis*, and *Coloradisaurus brevis* (Apaldetti et al. 2013), whereas these sulci are either incipient or absent in *Blikanasaurus cromptoni* (SAM-PK-K403), *Eucnemesaurus fortis* (BP/1/6111; Yates 2007), *Jaklapallisaurus asymmetricus* (Ezcurra et al. 2023), *Melanorosaurus readi* (SAM-PK-3449), *Mussaurus patagonicus* (Otero and Pol 2013), *Riojasaurus incertus* (PVL 3808), and *Sefapanosaurus zastronensis* (BP/1/7445; Otero et al. 2015).

The cnemial crest of *Musankwa sanyatiensis* accounts for 23% of tibial length, as in *Macrocollum itaquii* (Müller et al. 2018), *Coloradisaurus brevis* (Apaldetti et al. 2013), and *Mussaurus patagonicus* (Otero and Pol 2013), whereas longer crests are present in *Blikanasaurus cromptoni* (31%, SAM-PK-K403; Galton and Van Heerden 1985), *Eucnemesaurus fortis* (29%, Van Hoepen 1920), *Melanorosaurus readi* (27%, SAM-PK-3449), and *Riojasaurus incertus* (31%, PVL 3808), with shorter crests in *Jaklapallisaurus asymmetricus* (19%, Ezcurra et al. 2023) and *Kholumolumo ellenbergerorum* (20%, Peyre de Fabrègues and Allain 2020). *Musankwa sanyatiensis* lacks the distinct intramuscular line that extends along the anterior surface of the distal tibial shaft in *Unaysaurus tolentinoi* Leal et al., 2004 (McPhee et al. 2020).

Blikanasaurus cromptoni (Galton and Van Heerden 1985) and *Mussaurus patagonicus* (Otero and Pol 2013) lack the foramen that is situated ventral to the base of the ascending process in *Musankwa sanyatiensis*, *Coloradisaurus brevis* (Apaldetti et al. 2013), *Riojasaurus incertus* (PVL 3808), *Unaysaurus tolentinoi* (McPhee et al. 2020), and many other early-diverging sauropodomorphs. The astragalus of *Musankwa sanyatiensis* lacks the diagnostic T-shaped ascending process of *Sefapanosaurus zastronensis* (BP/1/386; Otero et al. 2015). A distinct, deep concavity on the posteromedial surface of the ascending process is present in *Coloradisaurus brevis* (Apaldetti et al. 2013), *Musankwa sanyatiensis*, and *Riojasaurus incertus* (Novas 1989), but is absent in *Blikanasaurus cromptoni* (Galton and Van Heerden 1998) and *Mussaurus patagonicus* (Otero and Pol 2013). A prominent anteromedial process extends from

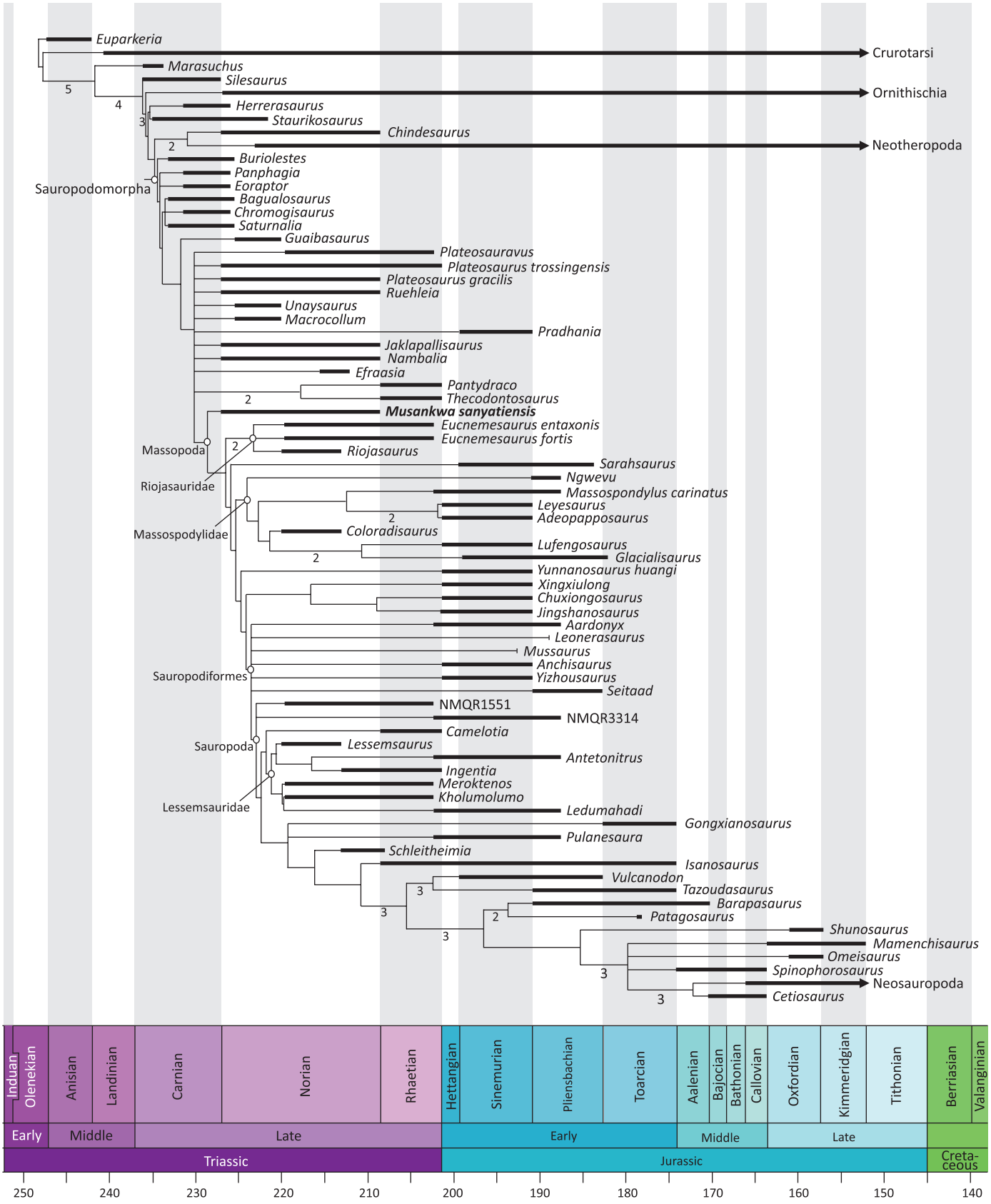

Fig. 4. Time-scaled reduced strict consensus of >10 000 MPTs with lengths of 1669 steps resulting from inclusion of *Musankwa sanyatiensis* gen. et sp. nov. (NHMZ 2521) in the dataset of Pol et al. (2021). Numbers below internal branches show Bremer supports for nodes with values >1. Further comments are provided in the text and the SOM 5. Time-scaling was conducted using the R package *strap* (Bell and Lloyd 2015).

the astragali of *Jaklapallisaurus asymmetricus* (Ezcurra et al. 2023), *Macrocollum itaquii* (Ezcurra et al. 2023), and *Unaysaurus tolentinoi* (McPhee et al. 2020) but is absent in *Musankwa sanyatiensis* and most other sauropodomorphs.

Although *Musankwa sanyatiensis* possesses no autapomorphies, which is perhaps unsurprising given the limited material available, the foregoing comparisons demonstrate that it can be distinguished from other Late Triassic massopodans, including all of its southern African contemporaries, on the basis of a unique character combination (see Diagnosis, above).

Stratigraphic and geographic range.—Type horizon and locality only.

Phylogenetic results

Our heuristic search strategy yielded >10 000 most parsimonious trees (MPTs) with lengths of 1669 steps, Consistency Index (CI) = 0.289, and Retention Index (RI) = 0.650. The reduced strict consensus of these trees (following a posteriori taxon deletion, see above) is relatively well-resolved, containing large polytomies only at the base of Sauropodomorpha (due to lability in the position of *Pampadromeus*) at the node subtending Massospoda (due to the instability of *Nambalia* and *Pradhania*) and at the base of Sauropoda (sensu Pol et al. 2021) (due to the lability of *Irisosaurus*). Bremer supports are generally low, with values of one or two for most nodes in the tree and none exceeding a value of three within the ingroup.

In the set of MPTs, NHMZ 2521 has a single most-parsimonious position, as sister-taxon to the clade containing Riojasauridae and later-branching massopodans such as massospondylids and sauropodiforms. This phylogenetic position posits NMMZ 2521 as the earliest-branching member of Massopoda, diverging immediately after taxa like *Unaysaurus*, *Macrocollum*, and *Plateosaurus* and earlier than Riojasauridae.

Discussion

Musanwka sanyantiensis gen. et sp. nov. represents only the fourth dinosaur to be named from Zimbabwe, following the descriptions of "*Syntarsus*" *rhodesiensis* Raath, 1969, *Vulcanodon karibaensis* Raath, 1972, and *Mbiresaurus raathi* Griffin et al., 2022, and is the first to be named from the Mid-Zambezi Basin in over 50 years. Its discovery, and other recent finds (e.g., Barrett et al. 2020, 2023; Sciscio et al. 2021a, b), highlight the potential of the region for further palaeontological discoveries, although the low-relief nature of the available outcrop along the shores of Lake Kariba (see Sciscio et al. 2021b) and the variable areal extent of these sites, which are controlled by annual fluctuations in lake volume (both natural and artificial), constrain opportunities to prospect and excavate.

Previous discoveries of sauropodomorphs from the Karoo-aged sediments of Zimbabwe include: small, Carnian-aged, early-diverging taxa (*Mbiresaurus*, Griffin et al. 2022); medium-sized massospondylids from a variety of strata ranging from ?Late Triassic–Early Jurassic in age (referred to various species of *Massospondylus*, e.g., Bond 1955, 1965; Cooper 1981, but note that the taxonomic status of this material requires reappraisal); and the large-bodied early sauropod *Vulcanodon* (Raath 1972; Cooper 1984). *Musankwa* adds to this diversity by demonstrating the presence of an early-diverging Late Triassic massopodan, an evolutionary "grade" not previously recorded from the region at this time. The Zimbabwean sauropodomorph assemblage is therefore similar to the mixture of sauropodomorph taxa known from the Elliot Formation of the MKB (McPhee et al. 2017), which yields species-rich faunas comprising early diverging massopodans and sauropodiforms (although very early diverging sauropodomorph taxa are currently unknown from the MKB). Similar mixtures of non-massopodans and massopodans also occur in the Late Triassic basins of South America (Pol et al. 2021) and India (Novas et al. 2011).

In all the trees recovered by our phylogenetic analyses, *Musankwa* is recovered as the earliest-branching massopodan (Fig. 4). Massopoda is supported by a single synapomorphy: Character 365, "0" to "1", proximal end of the tibia with a transverse to anteroposterior length ratio >0.7. A similarly broad proximal tibia is present in most non-sauropodiform massopodans, but this feature is reversed in *Massospondylus carinatus* Owen, 1854, and *Lufengosaurus huenei* Young, 1941.

However, given the incompleteness of many early-branching massopodan taxa it should be noted that minor changes in scoring have the potential to affect the branching orders of the lineages subtending this node. More complete material, and re-examination of the character scores assigned to these taxa, is required to stabilize relationships in this part of the tree. Synapomorphies supporting other nodes within Massopoda are listed in the SOM 5.

The phylogenetic analysis also reveals several other character state transformations that might be considered local autapomorphies of *Musankwa* when optimized onto the MPTs (see SOM 5). These include, for example, the presence of a pyramidal dorsal process on the posteromedial corner of the astragalus (Character 315, "0" to "1"), a feature that is homoplastic across the tree but that is present in many massospondylids.

Although the material of *Musankwa* is limited it offers some insights into early massopodan evolution. For example, it lacks the straighter femora that are typically present in more deeply-nested massopodans. Moreover, given the early-diverging positions of *Musankwa* and riojasaurids within Massopoda, it is tempting to speculate that Massopoda had its origin in Gondwana as all these taxa are either from southern Africa or South America. However, the lack of resolution outside Massopoda makes it difficult to

establish their ancestral area with certainty. Finally, it is potentially noteworthy that the limited material of *Musankwa* is strikingly similar to *Riojasaurus* and *Eucnemesaurus,* with all three of these taxa sharing the same overall gestalt and possessing several unusual features in common, such as the possession of a particularly well-developed posterior tubercle on the proximal end of the femur (see Comparisons, above). It is tempting to speculate that these taxa might form a clade of Norian-aged Gondwanan taxa, but the discovery of more complete specimens of *Musankwa* is necessary to test this hypothesis.

Conclusions

Musankwa sanyatiensis gen. et sp. nov. is a new sauropodomorph taxon from the Norian (Upper Triassic) Pebbly Arkose Formation of the Mid-Zambezi Basin, Zimbabwe. It is represented by an articulated partial hind limb and can be distinguished from all other Late Triassic southern African taxa on the basis of a unique character combination. Phylogenetic analysis recovers *Musankwa* as the earliest-branching massopodan sauropodomorph and it shares some features with riojasaurids that might prove to be of further interest if more material comes to light. *Musankwa* is only the fourth dinosaur to be named from the Karoo-aged basins of Zimbabwe and demonstrates the potential for further significant discoveries in the region.

Acknowledgements

In addition to the owners and crew of "Musankwa", mentioned above, we thank the other members of the 2017–2018 expeditions for their help and support in the field: Lucy and Patricia Broderick (Harare, Zimbabwe), Kathleen Dollman (European Synchrotron Radiation Facility, Grenoble, France), Steve and Wendy Edwards (Musango Safari Camp, Kariba, Zimbabwe), Rowan MacNiven (San Francisco, USA), Steve Tolan (Chipembele Wildlife Education Trust, Zambia) and Pia Viglietti (Field Museum, Chicago, USA). We thank Matusadona National Park for permission to work in the region under a permit obtained from the Research Council of Zimbabwe (RCZ 02849). Access to comparative material was facilitated by Zaituna Skosan (SAM, Cape Town, South Africa), Sifelani Jirah (BP, Johannesburg, South Africa) and Pablo Ortiz (PVL, Tucumán, Argentina). Gideon Chinamatria (BP, Johannesburg, South Africa) provided assistance with μCT-scanning. TNT is made freely available by the generosity of the Willi Hennig Society. Useful comments on a previous version of this contribution were received from Omar Regalado Fernández (Universität Tübingen, Tübingen, Germany) and Rodrigo Müller (Universidade Federal de Santa Maria, Santa Maria, Brazil), and we thank the handling editor (Daniel Barta, Oklahoma State University, Tahlequah, USA) for their assistance. PMB thanks the Science Innovation Fund of the Natural History Museum for funding; LS acknowledges the support of the Swiss National Science Foundation (project number: 192036); JNC and KEJC were funded by GENUS: the DSI-NRF Centre of Excellence in Palaeoscience and PAST (the Palaeontological Scientific Trust); and JNC was also funded by NRF-AOP grants 98800, 118794 and 136516.

References

Apaldetti, C., Pol, D., and Yates, A.M. 2013. The postcranial anatomy of *Coloradisaurus brevis* (Dinosauria: Sauropodomorpha) from the Late Triassic of Argentina and its phylogenetic implications. *Palaeontology* 56: 277–301.

Attridge, J. 1963. The Upper Triassic Karroo deposits and fauna of southern Rhodesia. *South African Journal of Science* 59: 242–247.

Barrett, P.M., Chapelle, K.E.J., Staunton, C.K., Botha, J., and Choiniere, J.N. 2019. Postcranial osteology of the neotype specimen of *Massospondylus carinatus* Owen, 1854 (Dinosauria: Sauropodomorpha) from the upper Elliot formation of South Africa. *Palaeontologia africana* 53: 114–178.

Barrett, P.M., Sciscio, L., Viglietti, P.A., Broderick, T.J., Suarez, C.A., Sharman, G. A., Jones, A. S., Munyikwa, D., Edwards, S. F., Chapelle, K.E.J., Dollman, K.N., Zondo, M., and Choiniere, J.N. 2020. The age of the Tashinga Formation (Karoo Supergroup) in the Mid-Zambezi Basin, Zimbabwe and the first phytosaur from mainland sub-Saharan mainland Africa. *Gondwana Research* 81: 445–460.

Barrett, P.M., Sciscio, L., Zondo, M., Broderick, T.J., Munyikwa, D., Viglietti, P.A., Edwards, S.F., Chapelle, K.E.J., Dollman, K.N., and Choiniere, J.N. 2023. Faunal change across the Triassic–Jurassic boundary: new insights from the Mid-Zambezi Basin of Zimbabwe. *The Anatomical Record* 306 (Supplement 1): 30–32.

Bell, M.A. and Lloyd, G.T. 2015. Strap: an R package for plotting phylogenies against stratigraphy and assessing their stratigraphic congruence. *Palaeontology* 58: 379–389.

Bonaparte, J.F. 1971. Los tetrapodos del sector superior de la Formacion Los Colorados, La Rioja, Argentina. *Opera Lilloana* 22: 5–183.

Bonaparte, J.F. 1978. *Coloradia brevis* n. g. et n. sp. (Saurischia, Prosauropoda), dinosaurio Plateosauridae de la Formacion Los Colorados, *Triásico superior de La Rioja, Argentina. Ameghiniana* 15: 327–332.

Bonaparte, J.F. and Vince, M. 1979. El hallazgo del primer nido de dinosaurios Triásicos, (Saurischia, Prosauropoda), Triásico Superior de Patagonia, Argentina. *Ameghiniana* 16: 173–182.

Bond, G. 1955. A note on dinosaur remains from the Forest Sandstone (Upper Karroo). *Occasional Papers of the National Museums of Southern Rhodesia* 2 (20): 795–800.

Bond, G. 1965. Some new fossil localities in the Karroo System of Rhodesia. *Arnoldia* 11 (2): 1–4.

Bond, G. and Falcon, R. 1973. The palaeontology of Rhodesia, with a section on the palynology of the Middle Zambezi Basin. *Rhodesia Geological Survey Bulletin* 70: 1–121.

Bond, G., Wilson, J.F., and Raath, M.A. 1970. Upper Karroo pillow lava and a new sauropod horizon in Rhodesia. *Nature* 227: 1339.

Bordy, E.M., Abrahams, M., Sharman, G.R., Viglietti, P.A., Benson, R.B.J., McPhee, B.W., Barrett, P.M., Sciscio, L., Condon, D., Mundil, R., Rademan, Z., Jinnah, Z., Clark, J.M., Suarez, C.A., Chapelle, K.E.J., and Choiniere, J.N. 2020. A chronostratigraphic framework for the upper Stormberg Group: implications for the Triassic–Jurassic boundary in southern Africa. *Earth-Science Reviews* 203: 103120.

Bordy, E.M., Segwabe, T., and Makuke, B. 2010. Sedimentology of the Upper Triassic–Lower Jurassic (?) Mosolotsane Formation (Karoo Supergroup), Kalahari Karoo Basin, Botswana. *Journal of African Earth Sciences* 58: 127–140.

Campione, N.E., Evans, D.C., Brown, C.M., and Carrano, M.T. 2014. Body mass estimation in non-avian bipeds using a theoretical conversion to quadruped stylopodial proportions. *Methods in Ecology and Evoluion* 5: 913–923.

Catuneanu, O., Wopfner, H., Eriksson, P.G., Cairncross, B., Rubidge, B.S., Smith, R.M.H., and Hancox, P.J. 2005. The Karoo basins of south-central Africa. *Journal of African Earth Sciences* 43: 211–253.

Chapelle, K.E.J. and Choiniere, J.N. 2018. A revised cranial description of *Massospondylus carinatus* Owen (Dinosauria: Sauropodomorpha) based on computed tomographic scans and a review of cranial characters for basal Sauropodomorpha. *PeerJ* 6: e4224.

Choiniere, J.N. and Barrett, P.M. 2015. A sauropodomorph dinosaur from the ?Early Jurassic of Lusitu, Zambia. *Palaeontologica africana* 49: 42–52.

Cooper, M.R. 1980. The first record of the prosauropod dinosaur *Euskelosaurus* from Zimbabwe. *Arnoldia* 9 (3): 1–17.

Cooper, M.R. 1981. The prosauropod dinosaur *Massospondylus carinatus* Owen from Zimbabwe: its biology, mode of life and phylogenetic significance. *Occasional Papers of the National Museums and Monuments of Rhodesia, Series B (Natural Sciences)* 6: 689–840.

Cooper, M.R. 1982. A mid-Permian to earliest Jurassic tetrapod biostratigraphy and its significance. *Arnoldia* 7 (9): 77–103.

Cooper, M.R. 1984. A re-assessment of *Vulcanodon karibaensis* Raath (Dinosauria: Saurischia) and the origin of the Sauropoda. *Palaeontologica africana* 25: 203–231.

Ezcurra, M.D., Müller, R.T., Novas, F.E., and Chatterjee, S. 2023. Osteology of the sauropodomorph dinosaur *Jaklapallisaurus asymmetricus* from the Late Triassic of central India. *In*: F.L. Pinheiro, F.A. Pretto, and L. Kerber (eds.), The Dawn of an Era: Comparative and Functional Anatomy of Triassic Tetrapods. *The Anatomical Record* 307 (4): 1093–1112.

Galton, P.M. and Van Heerden, J. 1985. Partial hindlimb of *Blikanasaurus cromptoni* n. gen. and n. sp., representing a new family of prosauropod dinosaurs from the Upper Triassic of South Africa. *Geobios* 18: 509–516.

Galton, P.M. and Van Heerden, J. 1998. Anatomy of the prosauropod dinosaur *Blikanasaurus cromptoni* (Upper Triassic, South Africa), with notes on the other tetrapods from the lower Elliot Formation. *Paläontologische Zeitschrift* 72: 163–177.

Gauffre, F.-X. 1993. The most recent Melanorosauridae (Saurischia, Prosauropoda), Lower Jurassic of Lesotho, with remarks on the prosauropod phylogeny. *Neues Jahrbuch für Geologie und Paläontologie, Monatschefte* 1993 (11): 648–654.

Goloboff, P.A. and Catalano, S.A. 2016. TNT version 1.5, including a full implementation of phylogenetic morphometrics. *Cladistics* 32: 221–238.

Greber, N.D., Davies, J.H., Gaynor, S.P., Jourdan, F., Bertrand, H., and Schaltegger, U. 2020. New high precision U-Pb ages and Hf isotope data from the Karoo large igneous province; implications for pulsed magmatism and early Toarcian environmental perturbations. *Results in Geochemistry* 1: 100005.

Griffin, C.T., Wynd, B.M., Munyikwa, D., Broderick, T., Zondo, M., Tolan, S., Langer, M.C., Nesbitt, S.J., and Taruvinga, H.R. 2022. Africa's oldest dinosaurs reveal early suppression of dinosaur distribution. *Nature* 609: 313–319.

Haughton, S.H. 1924. The fauna and stratigraphy of the Stormberg Series. *Annals of the South African Museum* 12: 323–497.

Holzförster, F., Stollhofen, H., and Stanistreet, I.G. 1999. Lithostratigraphy and depositional environments in the Waterberg-Erongo area, central Namibia, and correlation with the main Karoo Basin, South Africa. *Journal of African Earth Sciences* 29: 105–123.

Huene, F. von. 1932. Die fossile Reptil-Ordnung Saurischia, ihre Entwicklung und Geschichte. *Monographien zur Geologie und Paläontologie, Series 1* 4: 1–361.

Jones, D.L., Duncan, R.A., Briden, J.C., Randall, D.E., and MacNiocaill, C. 2001. Age of the Batoka basalts, northern Zimbabwe, and the duration of Karoo Large Igneous Province magmatism. *Geochemistry, Geophysics, Geosystems* 2 (2): 2000GC000110.

Kitching, J.W. and Raath, M.A. 1984. Fossils from the Elliot and Clarens formations (Karoo Sequence) of the Northeastern Cape, Orange Free State and Lesotho, and a suggested biozonation based on tetrapods. *Palaeontologica africana* 25: 111–125.

Knoll, F. 2004. Review of the tetrapod fauna of the "lower Stormberg Group" of the main Karoo Basin (southern Africa): implication for the age of the lower Elliot Formation. *Bulletin de la Sociéte géologique de France* 175: 73–83.

Knoll, F. 2005. The tetrapod fauna of the upper Elliot and Clarens formations in the main Karoo Basin (South Africa and Lesotho). *Bulletin de la Sociéte géologique de France* 176: 81–91.

Leal, L.A., Azevedo, S.A.K., Kellner, A.W.A., and Da Rosa, Á.A.S. 2004. A new early dinosaur (Sauropodomorpha) from the Caturrita Formation (Late Triassic), Paraná Basin, Brazil. *Zootaxa* 690: 1–24.

McPhee, B.W., Bittencourt, J.S., Langer, M.C., Apaldetti, C., and Da Rosa, Á.A.S. 2020. Reassessment of *Unaysaurus tolentinoi* (Dinosauria: Sauropodomorpha) from the Late Triassic (early Norian) of Brazil, with a consideration of the evidence for monophyly within non-sauropodan sauropodomorphs. *Journal of Systematic Palaeontology* 18: 259–293.

McPhee, B.W., Bordy, E.M., Sciscio, L., and Choiniere, J.N. 2017. The sauropodomorph biostratigraphy of the Elliot Formation of southern Africa: Tracking the evolution of Sauropodomorpha across the Triassic–Jurassic boundary. *Acta Palaeontologica Polonica* 62: 441–465.

McPhee, B.W., Choiniere, J.N., Yates, A.M., and Viglietti, P.A. 2015. A second species of *Eucnemesaurus* Van Hoepen, 1920 (Dinosauria, Sauropodomorpha): new information on the diversity and evolution of the sauropodomorph fauna of South Africa's lower Elliot Formation (latest Triassic). *Journal of Vertebrate Paleontology* 35 (5): e980504.

Miall, A.D. 2006. *The Geology of Fluvial Deposits: Sedimentary Facies, Basin Analysis, and Petroleum Geology*. 582 pp. Springer-Verlag, Berlin.

Miall, A.D. 2010. *The Geology of Stratigraphic Sequences. 2nd Edition.* 522 pp. Springer-Verlag, Berlin.

Munyikwa, D. 1997. Faunal analysis of Karoo-aged sediments in the northern Limpopo Valley, Zimbabwe. *Arnoldia* 10 (13): 129–140.

Müller, R.T., Langer, M.C., and Dias-da-Silva, S. 2018. An exceptionally preserved association of complete dinosaur skeletons reveals the oldest long-necked sauropodomorphs. *Biology Letters* 14 (11): 0633.

Novas, F.E. 1989. The tibia and tarsus in Herrerasauridae (Dinosauria, incertae sedis) and the origin and evolution of the dinosaurian tarsus. *Journal of Paleontology* 63: 677–690.

Novas, F.E., Ezcurra, M.D., Chatterjee, S., and Kutty, T.S. 2011. New dinosaur species from the Upper Triassic Upper Maleri and Lower Dharmaram formations of central India. *Earth and Environmental Science Transactions of the Royal Society of Edinburgh* 101: 333–349.

Otero, A. and Pol, D. 2013. Postcranial anatomy and phylogenetic relationships of *Mussaurus patagonicus* (Dinosauria: Sauropodomorpha). *Journal of Vertebrate Paleontology* 33: 1138–1168.

Otero, A., Krupandan, E, Pol, D., Chinsamy, A., and Choiniere, J.N. 2015. A new basal sauropodiform from South Africa and the phylogenetic relationships of basal sauropodomorphs. *Zoological Journal of the Linnean Society* 174: 589–634.

Owen, R. 1854. *Descriptive Catalogue of the Fossil Organic Remains of Reptilia and Pisces contained in the Museum of the Royal College of Surgeons*. 184 pp. Taylor and Francis, London.

Peyre de Fabrègues, C. and Allain, R. 2016. New material and revision of *Melanorosaurus thabanensis*, a basal sauropodomorph from the Upper Triassic of Lesotho. *PeerJ* 4: e1639.

Peyre de Fabrègues, C. and Allain, R. 2020. *Kholumolumo ellenbergerorum*, gen. et sp. nov., a new early sauropodomorph from the lower Elliot Formation (Upper Triassic) of Maphutseng, Lesotho. *Journal of Vertebrate Paleontology* 39 (6): e1732996.

Pol, D., Otero, A., Apaldetti, C., and Martínez, R.N. 2021. Triassic sauropodomorph dinosaurs from South America: the origin and diversification of dinosaur dominated herbivorous faunas. *Journal of South American Earth Sciences* 107: 103145.

Raath, M.A. 1969. A new coelurosaurian dinosaur from the Forest Sandstone of Rhodesia. *Arnoldia* 4 (28): 1–25.

Raath, M.A. 1972. Fossil vertebrate studies in Rhodesia: a new dinosaur (Reptilia: Saurischia) from near the Trias–Jurassic boundary. *Arnoldia* 5 (30): 1–37.

Raath, M.A. 1977. *The Anatomy of the Triassic Theropod* Syntarsus rhodesiensis *(Saurischia:Podokesauridae) and a Consideration of its Biology*. 364 pp. Ph.D. Dissertation, Rhodes University, Grahamstown.

Raath, M.A. 1996. The earliest evidence of dinosaurs from central Gondwana. *Memoirs of the Queensland Museum* 39: 703–709.

Raath, M.A., Oesterlen, P.M., and Kitching, J.W. 1992. First record of Triassic Rhychosauria (Reptilia: Diapsida) from the lower Zambezi Valley, Zimbabwe. *Palaeontologica africana* 29: 1–10.

Raath, M.A., Smith, C.C., and Bond, G. 1970. A new Upper Karroo dino-

saur fossil locality on the lower Angwa River, Sipolilo District, Rhodesia. *Arnoldia* 4 (35): 1–10.

Rogers, R.R., Curry Rogers, K., Munyikwa, D., Terry, R.C., and Singer, B.S. 2004. Sedimentology and taphonomy of the upper Karoo-equivalent Mpandi Formation in the Tuli Basin of Zimbabwe, with a new $^{40}Ar/^{39}Ar$ age for the Tuli basalts. *Journal of African Earth Sciences* 40: 147–161.

Sciscio, L., Broderick, T.J., Barrett, P.M., Munyikwa, D., Zondo, M., and Choiniere, J.N. 2021a. Invertebrate and plant trace fossils from the terrestrial Late Triassic of Zimbabwe. *Palaios* 36: 129–140.

Sciscio, L., Viglietti, P.A., Barrett, P.M., Broderick, T.J., Munyikwa, D., Chapelle, K.E.J., Dollman, K.N., Edwards, S.F., Zondo, M., and Choiniere, J.N. 2021b. Sedimentology and palaeontology of the Upper Karoo Group sediments in the Mid-Zambezi Basin, Zimbabwe: new localities and their implications for interbasinal correlation. *Geological Magazine* 158: 1035–1058.

Sues, H.-D., Reisz, R.R., Hinic, S., and Raath, M.A. 2004. On the skull of *Massospondylus carinatus* Owen, 1854 (Dinosauria: Sauropodomorpha) from the Elliot and Clarens formations (Lower Jurassic) of South Africa. *Annals of the Carnegie Museum* 73: 239–257.

Van Hoepen, E.C.N. 1920. Contributions to the knowledge of the reptiles of the Karroo Formation. 6. Further dinosaurian material in the Transvaal Museum. *Annals of the Transvaal Museum* 7 (2): 93–141.

Viglietti, P.A., Barrett, P.M., Broderick, T.J., Munyikwa, D., MacNiven, R., Broderick, L., Chapelle, K.E.J., Glynn, D., Edwards, S., Zondo, M., Broderick, P., and Choiniere, J. N. 2018. Stratigraphy of the *Vulcanodon* type locality and its implications for regional correlations within the Karoo Supergroup. *Journal of African Earth Sciences* 137: 149–156.

Viglietti, P.A., McPhee, B.W. Bordy, E.M., Sciscio, L., Barrett, P.M., Benson, R.B.J., Wills, S., Chapelle, K.E.J., Dollman, K.N., Mdekazi, C., and Choiniere, J.N. 2020a. Biostratigraphy of the *Massospondylus* Assemblage Zone (Stormberg Group, Karoo Supergroup), South Africa. *South African Journal of Geology* 123: 249–262.

Viglietti, P. A., McPhee, B.W. Bordy, E.M., Sciscio, L., Barrett, P.M., Benson, R.B.J., Wills, S., Tolchard, F., and Choiniere, J.N. 2020b. Biostratigraphy of the *Scalenodontoides* Assemblage Zone (Stormberg Group, Karoo Supergroup), South Africa. *South African Journal of Geology* 123: 239–248.

Yates, A.M. 2003. A definite prosauropod dinosaur from the Lower Elliot Formation (Norian: Upper Triassic) of South Africa. *Palaeontologia africana* 39: 63–68.

Yates, A.M. 2007. Solving a dinosaurian puzzle: the identity of *Aliwalia rex* Galton. *Historical Biology* 19: 93–123.

Young, C.-C. 1941. A complete osteology of *Lufengosaurus huenei* Young (gen. et sp. nov.) from Lufeng, Yunnan, China. *Palaeontologica Sinica, Series C* 7: 1–53.